Science of the Total Environment 616–617 (2018) 363–375

Contents lists available at ScienceDirect

Science of the Total Environment

journal homepage: www.elsevier.com/locate/scitotenv

A new method and a new index for identifying socioeconomic drought events under climate change: A case study of the East River basin in China

Haiyun Shi [a,b], Ji Chen [a,*], Keyi Wang [c], Jun Niu [d,e]

[a] Department of Civil Engineering, The University of Hong Kong, Hong Kong, China
[b] State Key Laboratory of Plateau Ecology and Agriculture, Qinghai University, Xining, Qinghai, China
[c] State Key Laboratory of Hydroscience & Engineering, Tsinghua University, Beijing, China
[d] Center for Agricultural Water Research in China, China Agricultural University, Beijing, China
[e] College of Water Resources & Civil Engineering, China Agricultural University, Beijing, China

HIGHLIGHTS

- Development of a heuristic method for identifying socioeconomic drought events
- A new index, the socioeconomic drought index (SEDI), is proposed.
- Historical and future drought analyses under climate change are conducted.
- The impact of reservoir operation on drought analysis is discussed.

GRAPHICAL ABSTRACT

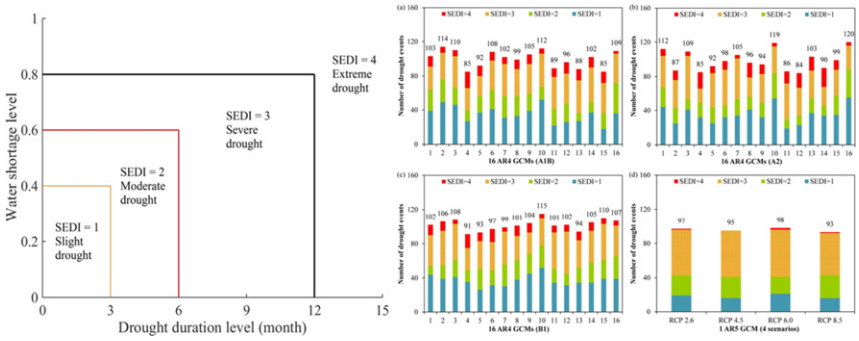

ARTICLE INFO

Article history:
Received 30 August 2017
Received in revised form 30 October 2017
Accepted 30 October 2017
Available online 7 November 2017

Editor: Ouyang Wei

Keywords:
A heuristic method
Socioeconomic drought index (SEDI)
Climate change
VIC model
Reservoir operation
East River basin

ABSTRACT

Drought is a complex natural hazard that may have destructive damages on societal properties and even lives. Generally, socioeconomic drought occurs when water resources systems cannot meet water demand, mainly due to a weather-related shortfall in water supply. This study aims to propose a new method, a heuristic method, and a new index, the socioeconomic drought index (SEDI), for identifying and evaluating socioeconomic drought events on different severity levels (i.e., slight, moderate, severe, and extreme) in the context of climate change. First, the minimum in-stream water requirement (MWR) is determined through synthetically evaluating the requirements of water quality, ecology, navigation, and water supply. Second, according to the monthly water deficit calculated as the monthly streamflow data minus the MWR, the drought month can be identified. Third, according to the cumulative water deficit calculated from the monthly water deficit, drought duration (i.e., the number of continuous drought months) and water shortage (i.e., the largest cumulative water deficit during the drought period) can be detected. Fourth, the SEDI value of each socioeconomic drought event can be calculated through integrating the impacts of water shortage and drought duration. To evaluate the applicability of the new method and new index, this study examines the drought events in the East River basin in South China, and the impact of a multi-year reservoir (i.e., the Xinfengjiang Reservoir) in this basin on drought analysis is also investigated. The historical and future streamflow of this basin is simulated using a hydrologic model, Variable Infiltration Capacity (VIC) model. For historical and future drought analysis, the proposed new method and

* Corresponding author.
E-mail address: jichen@hku.hk (J. Chen).

https://doi.org/10.1016/j.scitotenv.2017.10.321

index are feasible to identify socioeconomic drought events. The results show that a number of socioeconomic drought events (including some extreme ones) may occur in future, and the appropriate reservoir operation can significantly ease such situation.

1. Introduction

Drought is regarded as a complex natural hazard that occurs in large areas over long time periods and may have highly destructive effects on a number of aspects, such as water supply, agricultural production, and ecological environment (e.g., Gan et al., 2016; Yoo et al., 2016; Cammalleri et al., 2017). Generally, drought can be classified into four categories, including meteorological drought, agricultural drought, hydrological drought, and socioeconomic drought (Wilhite and Glantz, 1985; American Meteorological Society, 2013). Meteorological drought is often defined as a lack of precipitation over a region for a period of time; agricultural drought links various characteristics (e.g., soil moisture) of meteorological drought to agricultural impacts; hydrological drought is concerned with the effects of dry periods on surface or subsurface hydrology and water resources; socioeconomic drought is usually associated with supply of and demand for an economic good (water), which can also incorporate features of meteorological, agricultural, and hydrological droughts (Kifer and Steward, 1938; Wilhite and Glantz, 1985; Mishra and Singh, 2010). The former three have attracted the attentions of many researchers (e.g., Guttman, 1998; Heim, 2002; Narasimhan and Srinivasan, 2005; Shukla and Wood, 2008; Mishra and Singh, 2010; Morán-Tejeda et al., 2013; Moorhead et al., 2015; Serinaldi, 2016; Lin et al., 2017; Wu et al., 2017); however, to the best of our knowledge, it is only until recently that there have been a few studies focusing on socioeconomic drought (e.g., Eklund and Seaquist, 2015; Mehran et al., 2015; Huang et al., 2016), which occurs when water resources systems cannot meet water demand due to a weather-related shortfall in water supply (American Meteorological Society, 2013). A drought can be quantified at different levels of water deficiency, but it is difficult to identify a drought event through comprehensively evaluating both water shortage and drought duration. Therefore, it is still a challenging task to develop such a new method and a new index for rationally identifying drought events.

In the past several decades, numerous drought indices have been developed based on different parameters (e.g., Heim, 2002; Mishra and Singh, 2010; Moorhead et al., 2015; Etienne et al., 2016; Ndehedehe et al., 2016). For example, Palmer (1965) proposed the Palmer Drought Severity Index (PDSI) based on precipitation, reference evapotranspiration and soil characteristics, which could be used for evaluating the meteorological anomaly at a variety of time scales; Karl (1986) further developed the Palmer Hydrological Drought Index (PHDI) to better treat the beginning and ending times of droughts. The Standardized Precipitation Index (SPI), originated by McKee et al. (1993) based on only precipitation, is also a popular tool to investigate drought occurrence. Sivakumar et al. (2011) developed the Relative Water Deficit (RWD) using actual and potential evapotranspiration as inputs. Moreover, drought indices, such as Crop Moisture Index (CMI) (Palmer, 1968), Surface Water Supply Index (SWSI) (Shafer and Dezman, 1982), Vegetation Condition Index (VCI) (Kogan, 1995), and Standardized Precipitation-Evapotranspiration Index (SPEI) (Vicente-Serrano et al., 2010), are all widely-used. However, all the above indices are used for assessing the effects of meteorological (e.g., PDSI, SPI and SPEI), hydrological (e.g., PHDI and SWSI) and agricultural (e.g., CMI, RWD and VCI) droughts. Moreover, these indices may have their own advantages and disadvantages. For example, SPI can be calculated for a variety of time scales, but the length of precipitation record and nature of probability distribution play a vital role in calculating SPI. PDSI is the first comprehensive index to assess the total moisture status of a region, but some rules (e.g., assuming that all precipitation is rain) to establish PDSI are arbitrary and PDSI is sensitive to precipitation and temperature (Mishra and Singh, 2010). SWSI is regarded to be complementary to PDSI, which has the synonymous scale with that used for PDSI and can monitor the impacts of hydrological droughts on urban and industrial water supplies, irrigation and hydroelectric power generation; however, the weights of the factors may vary with spatial scales and temporal scales due to differences in hydroclimatic variability (Wilhite and Glantz, 1985; Heim, 2002; Mishra and Singh, 2010). CMI is used as an indicator of the availability of moisture to meet short-term crop needs, but there is unnatural response to changes in temperature because of the dependence of the abnormal evapotranspiration term on the magnitude of potential evapotranspiration (Juhasz and Kornfield, 1978; Wilhite and Glantz, 1985; Mishra and Singh, 2010).

Due to continuous population growth, water demand has increased multifold and will keep increasing in future, probably causing more socioeconomic drought events around the world (Chen et al., 2016; Smirnov et al., 2016; Trinh et al., 2017). For this category of drought which is the least investigated, Mehran et al. (2015) proposed the Multivariate Standardized Reliability and Resilience Index (MSRRI) for assessing water stress due to both climatic conditions and local reservoir levels, and Huang et al. (2016) applied this index to examine the evolution characteristics of socioeconomic droughts in the Heihe River basin in China. However, this index only focuses on water shortage but does not include drought duration, which may also have crucial influences on drought analysis. Thus, it is vital to develop a new index for identifying socioeconomic drought events through integrating both water shortage and drought duration, especially in the context of climate change.

Climate change has been recognized as one of the major factors that have great impacts on drought (e.g., Hanson and Weltzin, 2000; Aherne et al., 2006; Hirabayashi et al., 2008; Ahn et al., 2016; Gizaw and Gan, 2017; Linares et al., 2017; Tietjen et al., 2017). Even a small change in climate may cause a dramatic change in hydrological cycle, leading to more frequent hydrological extremes (e.g., Pilling and Jones, 2002; Chen et al., 2011; Vicuna et al., 2013; Gu et al., 2015; Shi and Wang, 2015; Hoang et al., 2016; Shi et al., 2016a, 2017a). Globally, IPCC (Intergovernmental Panel on Climate Change) (2013) reported that the averaged land and ocean surface temperature had a warming of 0.85 °C over the period of 1880–2012 and a fast warming trend of 0.12 °C/decade over the period of 1951–2012. Regionally, a remarkable warming trend has been found in South China (e.g., Chen et al., 2011; Chan et al., 2012; Lau and Ng, 2013). Fischer et al. (2013) projected climate extremes in the Pearl River basin for the period of 2011–2050 using the daily output from the regional climate model COSMO-CLM, and the results indicated that warmer and drier conditions could be expected in the western and eastern parts, especially in summer and autumn.

In recent years, we have conducted several studies on climate change over the Pearl River basin (e.g., Niu, 2013; Niu and Chen, 2014, 2016; Niu et al., 2014, 2015, 2017). Niu and Chen (2014) investigated the terrestrial hydrological responses to precipitation variability over the West River basin with emphasis on an extreme drought event. Niu et al. (2014) revealed that the teleconnections between two climatic patterns (El Niño-Southern Oscillation, ENSO, and Indian Ocean Dipole, IOD) and hydrological variability, served as a reference for inferences on the occurrence of extreme hydrological events over the Pearl River basin. Niu et al. (2015) examined the spatio-temporal and evolution

features of drought events over the West River basin, and showed the differences of meteorological, hydrological and agricultural droughts.

Based on the above previous studies, this study aims to develop a new method, a heuristic method, and a new index, socioeconomic drought index (SEDI), for identifying socioeconomic drought events on different severity levels (i.e., slight, moderate, severe and extreme) through comprehensively evaluating the impacts of both water shortage and drought duration under climate change. Considering the gap between water supply and water demand, streamflow is adopted as the principal input in the new method and index. Historical drought analysis is conducted using the observed data, which can validate the applicability of the new method and index, and future drought analysis is conducted using different datasets of climate change scenarios, which can reflect a variety of drought conditions in future. Moreover, the impact of dam (and related reservoir) construction on drought analysis will be discussed in this study. Overall, the proposed method and index (SEDI) can provide a better understanding of socioeconomic drought under climate change, which will be valuable for decision-makers to synthetically evaluate the impacts of climate change and hydraulic structures on water resources management.

2. Methodology

2.1. The heuristic method and the SEDI

For a designated river basin, the heuristic method and the SEDI are developed as follows (see Fig. 1). First, the minimum in-stream water requirement (noted as MWR hereafter) (see Section 2.2 for details) of the river basin, which is enough to sustain and support the different functions in this river basin, is adopted as the threshold value through comprehensively considering a number of factors such as water quality, ecology, navigation, water supply and so on. Second, the monthly streamflow data, either the observed data recorded at the hydrological stations or the simulated data derived from the Variable Infiltration Capacity (noted as VIC hereafter) model (Liang et al., 1994) (see Section 2.3 for details), are used to identify drought month. Then, the monthly difference, which is the monthly streamflow data minus the MWR, is calculated. In this study, if the monthly difference is smaller than 0 (i.e., water deficit), the corresponding month will be regarded as a drought month. Third, according to the cumulative water deficit derived from the monthly water deficit, drought duration (i.e., the number of continuous drought months) and water shortage (i.e., the largest cumulative water deficit during the drought period) can be identified. It is worth noting that a socioeconomic drought event will continue until the cumulative water deficit turns into a non-negative value. Finally, for each identified socioeconomic drought event, the SEDI value can be calculated through integrating the impacts of water shortage and drought duration, which are classified into four different levels (see Table 1). It is worth noting that the indicators related to experiment procedures (e.g., the MWR value) may vary with land use and land cover dynamic, catchment geomorphology and scale, and even some climate-related events occurred in a particular region. Therefore, the proposed method and index are region-dependent, which indicates that the values of the indicators should be recalculated for different regions.

In this study, the four drought duration levels (DDLs) are defined as follows. The DDL value will be 1, 2, or 3 if the identified drought event is at the quarterly (i.e., 1–3 months), semi-annual (i.e., 4–6 months) or annual (i.e., 7–12 months) scale, respectively, and the DDL value will be 4 if the identified drought event lasts for more than a year (Table 1). In addition, the four water shortage levels (WSLs) are defined by a typical reservoir storage percentage (noted as RSP hereafter). In this study, the typical reservoir storage (noted as TRS hereafter) refers to the total manageable storage capacity of the reservoirs in a study area, and then the RSP can be calculated as the absolute value of the largest cumulative water deficit (noted as LCWD) divided by the TRS (Denver Water, 2002).

$$\mathrm{RSP} = \frac{\mathrm{Abs(LCWD)}}{\mathrm{TRS}} \tag{1}$$

where Abs() is the function of taking the absolute value. The WSL value will be 1, 2, or 3 if the RSP value is <40%, 60% or 80%, respectively, and if the RSP value is larger than 80%, the WSL value will be 4 (Table 1).

Therefore, for each identified socioeconomic drought event, the SEDI is defined in terms of the DDL and WSL values (see the equation below).

$$\mathrm{SEDI} = \max\{\mathrm{DDL}, \mathrm{WSL}\} \tag{2}$$

For example, if the WSL and DDL values are 2 and 3, the SEDI value will be 3, which means it is a severe socioeconomic drought event (Table 1). Fig. 2 shows the ranges of different SEDI values classified by different levels of water shortage and drought duration. Consequently,

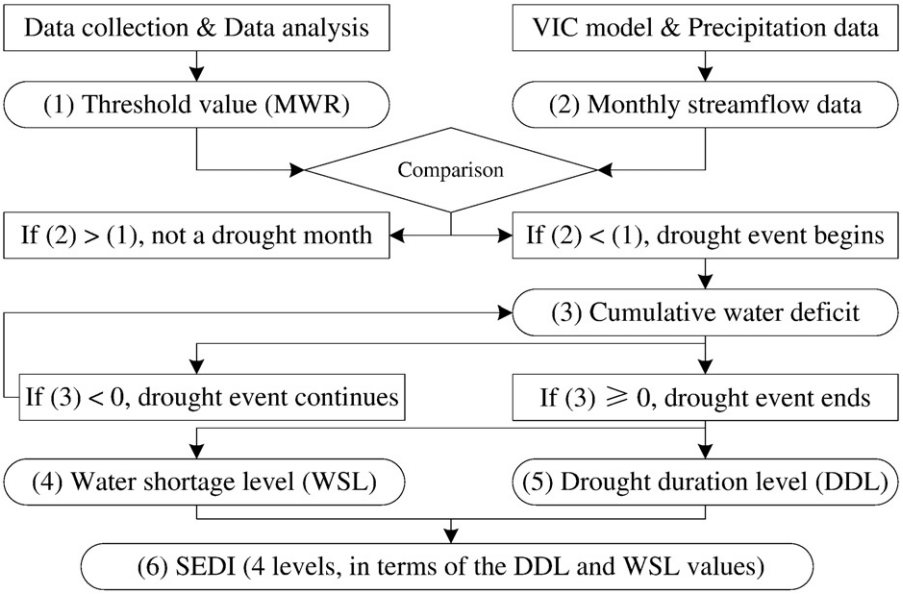

Fig. 1. Flowchart of the development of the heuristic method and the SEDI.

Table 1
Definitions of the SEDI based on different levels of water shortage and drought duration.

SEDI		Water shortage level (WSL)		Drought duration level (DDL)	
Value	Definition	Value	Definition	Value	Definition
1	Slight	1	RSP < 40%	1	Quarterly (i.e., 1–3 months)
2	Moderate	2	40% < RSP < 60%	2	Semi-annual (i.e., 4–6 months)
3	Severe	3	60% < RSP < 80%	3	Annual (i.e., 7–12 months)
4	Extreme	4	RSP ≥ 80%	4	>12 months

historical and future drought analyses can be conducted based on the proposed heuristic method and the SEDI.

Furthermore, to discuss the impact of reservoir operation on drought analysis, the following method is adopted. For a designated reservoir, there should be an upper bound of stored water (e.g., the effective storage of the reservoir) during the flood season limited by the requirement of flood control, which is also the available water volume remaining in the reservoir at the end of the flood season. Then, using the previously obtained monthly differences, the available water volume in the reservoir at the end of each month can be calculated by subtracting the monthly difference of that month from the available water volume in the reservoir at the end of the last month. In this study, if the available water volume turns into a negative value, it indicates that there will not be sufficient water even if the usable capacity (e.g., the effective storage) of the reservoir is run out.

2.2. The MWR value

The MWR is a critical variable in determining the drought occurrence and duration, and its value can be calculated as follows (Wu and Chen, 2013):

$$\mathrm{MWR} = \max\{Q_1, Q_2, Q_3, Q_4\} + Q_s \quad (3)$$

where Q_1 is the minimum streamflow required for maintaining water quality standard, Q_2 is the minimum ecological streamflow, Q_3 is the minimum streamflow for navigation, and Q_4 is the minimum streamflow for arresting seawater intrusion into the estuary. Q_s is the required pumping rate for the water supply to meet the regional water demand. In this study, Q_s is estimated using a five-stage water demand projection model proposed by Chen et al. (2015), which can project the future water demand in a designated region under the high, medium, and low projection scenarios, respectively. This five-stage

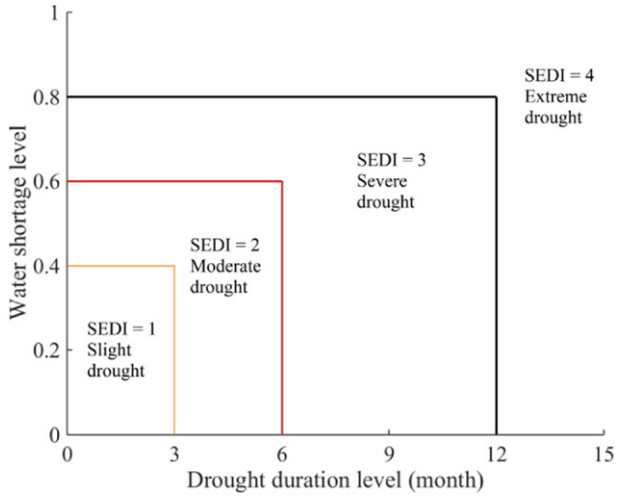

Fig. 2. The ranges of different SEDI values classified by different levels of drought duration and water shortage.

model uses the per capita gross domestic product based on purchasing power parity (noted as PPP GDP hereafter) and population as the main indicators to project future water demand. The PPP GDP serves as the indicator to identify the historic, current, and future water demand stages, which is the guide for water demand patterns, and population serves as the most important influencing factor for total water demand. Then, the regression equations to estimate the future water demand can be obtained (Chen et al., 2015). It is worth noting that the reasonable threshold value for the utilization ratio of water resources of a river is 30%, and the limiting threshold value is 40% (UN, 1997; Zuo, 2011). In other words, if >40% of river discharge is utilized, a critical situation regarding water scarcity exists while making use of <30% of river discharge can be regarded as sustainable and acceptable. As a result, the value of Q_s should not be larger than 30% of river discharge.

2.3. VIC model

One of representative land surface hydrological models, the VIC model (Liang et al., 1994), is a semi-distributed model, which maintains both surface energy and water balances over a grid cell, with its resolutions ranging from a fraction of a degree to several degrees latitude by longitude. The application of the sub-gird parameterization of the spatial variability of infiltration capacity in the VIC model makes it possible to represent the land surface hydrological processes at higher horizontal resolutions.

The VIC model has been applied to several large river basins (e.g., Nijssen et al., 2001). The high temporal resolution model forcing datasets and the global soil and vegetation datasets facilitate simulations and assessments of the global and regional land surface hydrological processes by the VIC model. The characteristics of global surface soil moisture fluxes at daily scale for the period of 1979–1993 were explored by the VIC model (Nijssen et al., 2001). The VIC model was applied to the East River basin for exploring the land surface hydrological features (Chen and Wu, 2008). Niu and Chen (2010) validated the streamflow simulations in the Pearl River basin with the streamflow observations from six hydrologic stations. Furthermore, Niu et al. (2014) further validated the streamflow simulations in the Pearl River basin with the streamflow observations from four more hydrologic stations. Overall, the VIC simulation of streamflow over the Pearl River basin is comparable to the observations. As a result, the parameters in the VIC model and the related routing model, which can be acquired from the previous studies (Chen and Wu, 2008; Niu and Chen, 2010; Niu et al., 2014), are directly used to simulate the future streamflow using climate projection scenarios which are downscaled from the outputs of General Circulation Models (GCMs) in this study. It is worth noting that there is no need to calibrate the VIC model for simulations at the monthly scale, with the acceptable simulation accuracy in the study basin. For running the VIC model, the soil and vegetation parameters are extracted from two global datasets (Nijssen et al., 2001).

2.4. Trend test method

In order to investigate the trends of the simulated future streamflow using different climate change scenarios, the Mann-Kendall trend test method is adopted. A number of previous studies have shown the robustness of this method as well as its wide application in the fields

such as meteorology, hydrology, and sedimentology (e.g., Croitoru et al., 2012; Manzanas et al., 2014; Shi and Wang, 2015; Shi et al., 2016b, 2017b).

The Mann-Kendall trend test is a non-parametric rank-based statistical test that was first proposed by Mann (1945) and further developed by Kendall (1975). Based on the Mann-Kendall trend test method, the slope of the series can be computed using the Thiel-Sen method (Thiel, 1950; Sen, 1968).

$$\beta = Median\left(\frac{X_j - X_i}{j - i}\right), for\ all\ i<j \tag{4}$$

where X_j and X_i are the observed values in the j-th and i-th year ($j > i$), respectively.

Moreover, prewhitening (von Storch and Navarra, 1995) is required to eliminate the influence of autocorrelation because such series is not applicable for the Mann-Kendall trend test method.

$$Xp_i = X_{i+1} - rX_i \tag{5}$$

where Xp_i is the observed value in the i-th year after prewhitening and r is the first-order autocorrelation coefficient of the series.

3. Study area and research data

3.1. Study area

The study area is the East River, a tributary of the Pearl River, which is the most important source of fresh water for Hong Kong (Niu and Chen, 2010). Therefore, to explore the status of water resources in this river basin is essential for evaluating water security of Hong Kong. The East River originates in the Xunwu county of Jiangxi Province, China, and its drainage area is 27,040 km^2, accounting for 5.96% of the total area of the Pearl River basin (PRWRC, 2005). The main stream of the East River flows from northeast to southwest (see Fig. 3), and the long-term annual average discharge in the East River is 23.8 km^3 (~755 m^3/s). The upper reach, named the Xunwushui River, flows towards the southwest and joins the Anyuanshui River in the Longchuan County, and from thereon it is named the East River. It is worth noting that the river channel in the mountainous upstream area of the East River is shallow and narrow, while the river channels in the middle and downstream areas can be used for navigation. Moreover, the Xinfengjiang (noted as XFJ hereafter) Reservoir, a multi-year reservoir

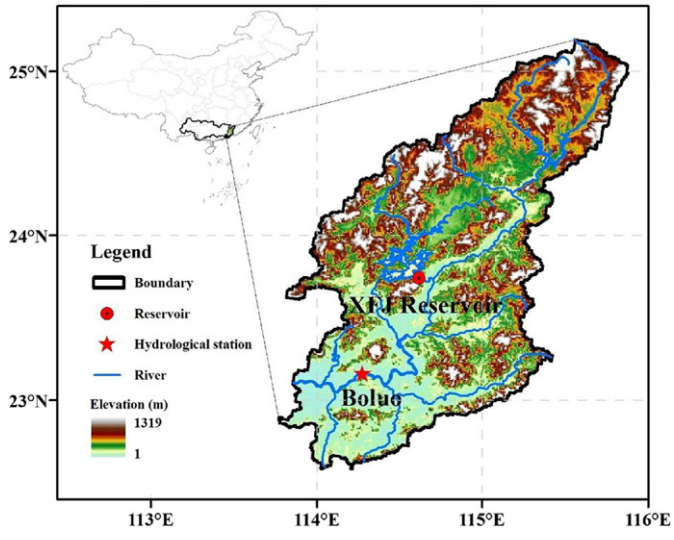

Fig. 3. The Xinfengjiang (XFJ) Reservoir and the Boluo hydrological station in the East River basin.

located in the East River basin, was completed in 1962. The total reservoir storage capacity is 13.9 km^3, among which 3.1 km^3 is the flood control storage, 6.5 km^3 is the effective storage, and 4.3 km^3 is the dead storage (Wu and Chen, 2012, 2013). In our previous studies, Niu (2013) examined the temporal patterns of precipitation and the influence of large-scale climate, and found a number of abnormal precipitation events during 1955–1975, 1980–1985, and 1990–1995 in the East River basin. Moreover, regarding dam (and related reservoir) construction as the best option to increase available water resources by storing water in the reservoir and to enhance the capabilities in water resources management (Chen et al., 2016), we have also proposed an operation-based scheme for a multi-year and multi-purpose reservoir (Wu and Chen, 2012), an improved method for irrigation water demand estimation, and an optimization method for reservoir operation (Wu and Chen, 2013).

3.2. Research data

In this study, the projected precipitation datasets derived from different climate change scenarios are the outputs from 17 GCMs, including 16 IPCC AR4 (the Fourth Assessment Report) GCMs during 1951–2099 and 1 IPCC AR5 (the Fifth Assessment Report) GCM during 2000–2099 (see Table 2). The selected AR4 GCMs used three scenarios (Special Report on Emissions Scenario, SRES A2/A1B/B1) to project future climate change, and assumptions were made about how factors driving emissions (e.g., population growth, economic development and advances in technology) would change in future (IPCC, 2007). Moreover, the selected AR5 GCM adopted four new scenarios (Representative Concentration Pathway, RCP 2.6/4.5/6.0/8.5). Instead of making assumptions about how factors driving emissions might change, each RCP scenario expressed a different total radiative forcing by 2100 or how much extra energy the earth would retain as a result of human activities (IPCC, 2013). The GCM outputs can be obtained from the World Climate Research Programme (WCRP) CMIP3 multi-model dataset (Meehl et al., 2007). These data have been downscaled to a 0.5° grid using the bias-correction/spatial downscaling method (Wood et al., 2004; Maurer et al., 2009), based on the gridded observations during 1950–1999 (Adam and Lettenmaier, 2003). With the 52 ($=16 \times 3 + 4$) projected precipitation datasets, the monthly streamflow data used for drought analysis can be simulated using the VIC model. In addition, the observed monthly streamflow data recorded at the Boluo station (see Fig. 3) in the East River basin during 1954–1988 are collected.

To delineate the East River basin, GTOPO30 DEM dataset with 1000 m spatial resolution is used (see Fig. 3). The VIC model is run at the daily scale with $0.5° \times 0.5°$ spatial resolution to provide the simulated streamflow, and the soil and vegetation data over this river basin are extracted from the global soil and vegetation datasets (Nijssen et al., 2001).

4. Results and discussion

4.1. The MWR value of the East River basin

For the East River basin, the MWR value is calculated through considering the change of water demand in future. Following the previous studies (Wu et al., 2001; Lee et al., 2007), this study adopts the estimated values of Q_1, Q_2, Q_3, and Q_4 at the Boluo station as 317, 230, 210, and 150 m^3/s in 2010, respectively. Further, this study assumes that these values will not change along with time; therefore, the maximum value among Q_1, Q_2, Q_3, and Q_4 is 317 m^3/s. According to Lee et al. (2007), the estimated value of Q_s was 150 m^3/s in 2010; however, it is worth noting that water demand will increase along with population growth in future (Chen et al., 2016), leading to the change of the Q_s value, as well as the MWR value. Chen et al. (2015) projected the future water demand in the East River basin under the high, medium and low projection scenarios using a five-stage water demand projection model, and

Table 2
Summary of the 52 selected datasets.

Data source (climate model)	Emission scenarios	Horizontal resolution	Period
16 IPCC AR4 GCMs (1. bccr_bcm2_0.1, 2. ncar_ccsm3_0.1, 3. cccma_cgcm3_1.1, 4. cnrm_cm3.1, 5. csiro_mk3_0.1, 6. mpi_echam5.1, 7. miub_echo_g.1, 8. gfdl_cm2_0.1, 9. gfdl_cm2_1.1, 10. giss_model_e_r.1/2, 11. inmcm3_0.1, 12. ipsl_cm4.1, 13. miroc3_2_medres.1, 14. mri_cgcm2_3_2a.1, 15. ncar_pcm1.1/2, 16. ukmo_hadcm3.1)	SRES A2/A1B/B1	0.5° × 0.5°	1951–2099
1 IPCC AR5 GCM (17. HadGEM2-ES)	RCP 2.6/4.5/6.0/8.5	0.5° × 0.5°	2000–2099

the results showed that the annual water demand would keep increasing before 2070 and then decrease from 2070 to 2099 under the high and medium projection scenarios. According to the above mentioned assumption, the MWR value will have the same changing feature with the annual water demand in future. As a result, the MWR value of the East River basin for each year during 2010–2099 can be obtained (Fig. 4). In this study, the MWR values under the medium projection scenario from 2020 to 2099 are selected for future drought analysis, and the maximum Q_s value under this scenario (176 m^3/s) will occur in 2070. Because the long-term annual average river discharge in the East River is 755 m^3/s, the maximum Q_s value under this scenario accounts for 23.3% (=176/755) of the total river discharge, which can meet the requirement of <30% (Zuo, 2011).

4.2. Historical drought analysis

Due to data availability, the observed monthly streamflow data recorded at the Boluo station in the East River basin during 1954–1988 are collected in this study. Moreover, only the monthly streamflow data simulated using the 48 (=16 × 3) datasets from 16 GCMs and 3 AR4 scenarios are used for historical drought analysis. Fig. 5 shows the comparison of the mean value of the simulated streamflow data from the 48 datasets against the observations for each month during 1954–1988. Overall, the average values of the simulated streamflow data from the 48 datasets can match the historical observations; however, large differences appear in a few months. The reasons for this may be as follows: on the one hand, the monthly streamflow at the Boluo station is significantly influenced by the operation of the XFJ Reservoir (Niu and Chen, 2010; Wu and Chen, 2012), and Niu and Chen (2010) indicated that the model performance of streamflow simulation is satisfied before the operation of the XFJ Reservoir. On the other hand, in climate change study, the GCM outputs can be used to analyze natural multi-decadal climate variations, but cannot be used to confirm the exact extreme events occurred in a certain year (Teegavarapu, 2012).

Using the heuristic method and the SEDI proposed in Section 2.1, historical socioeconomic drought events are identified from the observed and simulated monthly streamflow data, respectively. For the observed monthly streamflow data, the SEDI value of the severest drought event over the period of 1954–1988 is 4, which can reach the level of an extreme drought. The identified socioeconomic drought event started in December 1962 and ended in May 1964, lasting for 18 months (i.e., DDL = 4); however, the RSP value of this drought event is only 0.37 (i.e., WSL = 1). In addition, based on the simulated monthly streamflow data, the SEDI value of the severest drought event over the period of 1954–1988 is 3, which indicates this is a severe drought. The identified socioeconomic drought event started in September 1962 and ended in May 1963, lasting for 9 months (i.e., DDL = 3); moreover, the RSP value of this drought event is 0.61 (i.e., WSL = 3). According to the historical records, the severest drought event during 1954–1988 indeed occurred around 1963 (Peart, 2004), which preliminarily proves the validity of the heuristic method and the SEDI for identifying the occurrence period of the socioeconomic drought event. However, the drought duration of the socioeconomic drought event identified from the observed data is longer, but the water shortage of the socioeconomic drought event identified from the simulated data is higher.

4.3. Future drought analysis

4.3.1. Trend analysis of the simulated streamflow in future

In this study, trend analysis of the simulated streamflow at the Boluo station during 2020–2099 is conducted at the annual scale. Using the Mann-Kendall trend test method, the trends of the annual streamflow data under all the 52 datasets are detected and Table 3 lists the relevant results. The trend slopes vary greatly among different scenarios, with the most significant decreasing trend of −2.77 mm/year in one GCM (i.e., mpi_echam5.1) under A1B scenario and the most significant increasing trend of 11.02 mm/year in another GCM (i.e., ukmo_hadcm3.1) under B1 scenario. There are 40 AR4 datasets (i.e., 12/13/15 under A1B/A2/B1

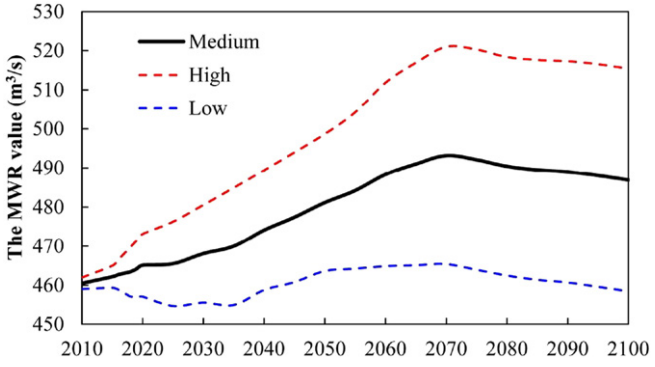

Fig. 4. The MWR value of the East River basin for each year during 2010–2099 under high, medium and low projection scenarios.

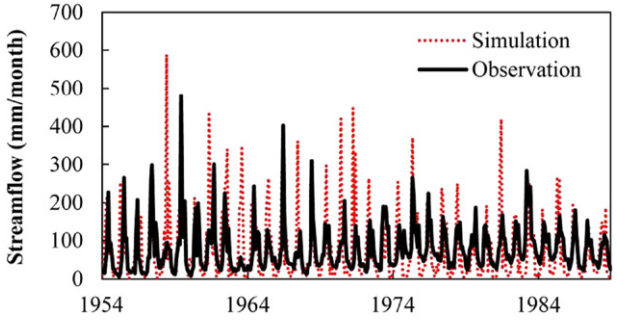

Fig. 5. Comparison of the mean value of the simulated streamflow data from the 48 datasets against the observations for each month during 1954–1988.

Table 3
The slopes (mm/year) of the simulated streamflow at the Boluo station during 2020–2099 for each of the 52 datasets. Note: p is the significance level.

AR4 scenario	A1B	A2	B1
1. bccr_bcm2_0.1	0.43 ($p > 0.1$)	0.11 ($p > 0.1$)	1.85 ($p > 0.1$)
2. ncar_ccsm3_0.1	2.57 ($p > 0.1$)	4.06 (***p*** < **0.05**)	1.65 ($p > 0.1$)
3. cccma_cgcm3_1.1	1.58 ($p > 0.1$)	0.03 ($p > 0.1$)	0.51 ($p > 0.1$)
4. cnrm_cm3.1	2.56 (***p*** < **0.1**)	2.02 ($p > 0.1$)	2.29 ($p > 0.1$)
5. csiro_mk3_0.1	−1.72 ($p > 0.1$)	−2.33 ($p > 0.1$)	0.49 ($p > 0.1$)
6. mpi_echam5.1	−2.77 (***p*** < **0.1**)	0.29 ($p > 0.1$)	0.27 ($p > 0.1$)
7. miub_echo_g.1	3.38 (***p*** < **0.05**)	1.51 ($p > 0.1$)	1.69 ($p > 0.1$)
8. gfdl_cm2_0.1	5.33 (***p*** < **0.01**)	1.08 ($p > 0.1$)	3.89 (***p*** < **0.05**)
9. gfdl_cm2_1.1	0.44 ($p > 0.1$)	3.03 (***p*** < **0.1**)	4.02 (***p*** < **0.05**)
10. giss_model_e_r.1/2	3.55 (***p*** < **0.1**)	4.28 (***p*** < **0.05**)	1.97 ($p > 0.1$)
11. inmcm3_0.1	3.73 (***p*** < **0.1**)	5.12 (***p*** < **0.05**)	−0.71 ($p > 0.1$)
12. ipsl_cm4.1	−2.22 ($p > 0.1$)	2.12 ($p > 0.1$)	3.27 (***p*** < **0.05**)
13. miroc3_2_medres.1	−2.45 ($p > 0.1$)	−0.03 ($p > 0.1$)	0.25 ($p > 0.1$)
14. mri_cgcm2_3_2a.1	3.04 (***p*** < **0.05**)	2.80 (***p*** < **0.1**)	5.95 (***p*** < **0.01**)
15. ncar_pcm1.1/2	2.45 ($p > 0.1$)	−0.39 ($p > 0.1$)	3.08 (***p*** < **0.1**)
16. ukmo_hadcm3.1	6.09 (***p*** < **0.01**)	6.75 (***p*** < **0.01**)	11.02 (***p*** < **0.01**)

AR5 scenario	RCP 2.6	RCP 4.5	RCP 6.0	RCP 8.5
17. HadGEM2-ES	2.04 (***p*** < **0.1**)	1.24 ($p > 0.1$)	2.63 (***p*** < **0.05**)	3.24 (***p*** < **0.05**)

scenarios) showing the increasing trends in the simulated annual streamflow, comparing to only 8 AR4 datasets (i.e., 4/3/1 under A1B/A2/B1 scenarios) showing the decreasing trends. However, 20 of the 40 (i.e., 50%) increasing trends are statistically significant ($p < 0.1$) while only 1 of the 8 (i.e., 12.5%) decreasing trends is statistically significant. In contrast, the increasing trends are found under all the four AR5 datasets, among which only the increasing trend under RCP 4.5 scenario is not statistically significant (see Table 3).

It is worth noting that more datasets show the increasing trends rather than the decreasing trends in the simulated streamflow at the annual scale. However, it does not mean that the drought conditions will be improved in future because of the non-uniformity of the streamflow among different months. In the following subsection, future drought analysis will be conducted at the monthly scale, focusing on the identification of socioeconomic drought events.

4.3.2. Identification of socioeconomic drought events in future

In consideration of the changing MWR values of the East River basin under medium projection scenarios during 2020–2099 (Fig. 4), socio-economic drought events in future are identified based on the monthly

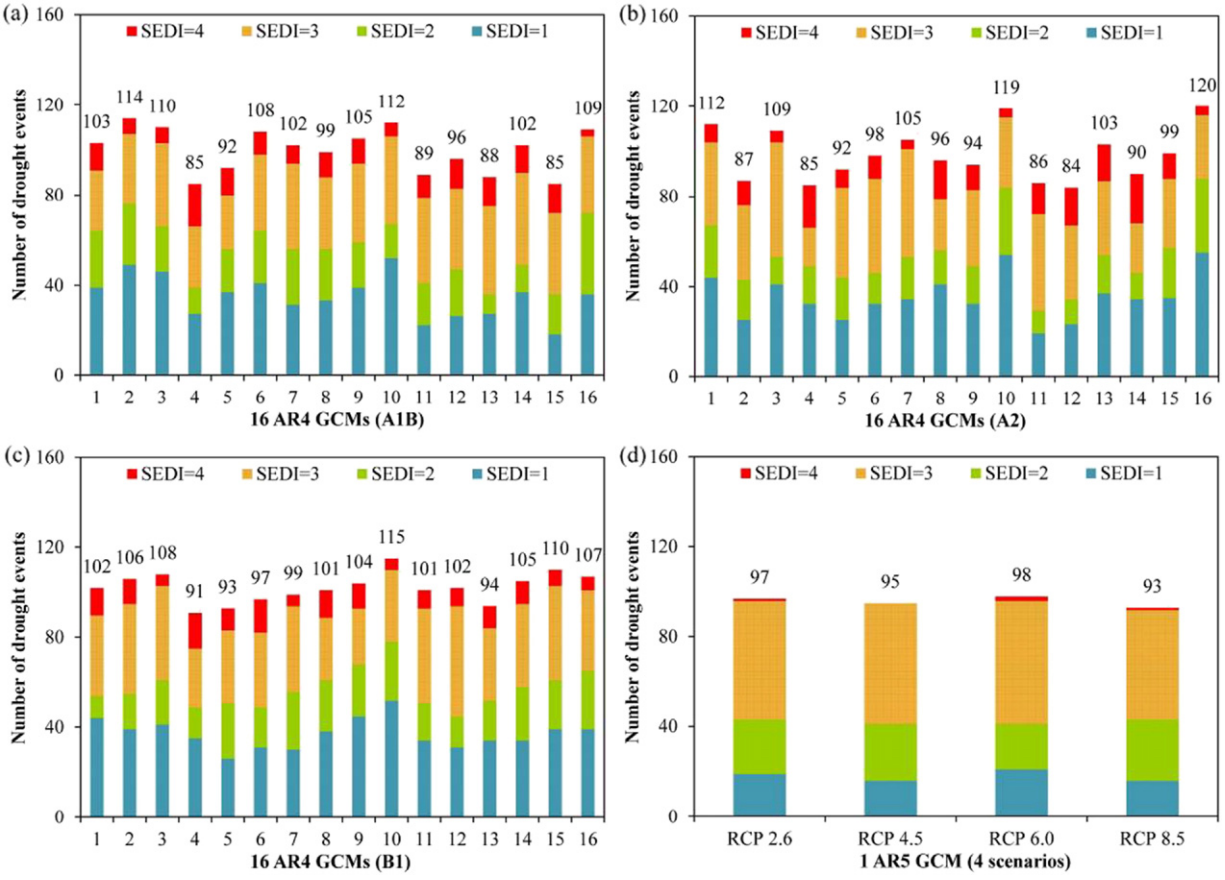

Fig. 6. The numbers of socioeconomic drought events with different SEDI values for each of the 52 datasets (16 AR4 GCMs under the three scenarios and 1 AR5 GCM under the four scenarios).

streamflow data simulated with 16 GCMs under the three AR4 emission scenarios and 1 GCM under the four AR5 scenarios.

First, the numbers of socioeconomic drought events with different SEDI values are identified for each of the 52 datasets, and the results are shown in Fig. 6. For the 16 GCMs, the results are rather different among different models under the three AR4 emission scenarios (i.e., SRES A1B/A2/B1). The total numbers of socioeconomic drought events vary between 85–114 under SRES A1B scenario, 84–120 under SRES A2 scenario and 91–115 under SRES B1 scenario, respectively. The mean values of the total numbers are more or less the same under the three emission scenarios (i.e., 100, 99 and 102 under SRES A1B, A2 and B1 scenarios, respectively). For the four AR5 scenarios (i.e., RCP 2.6/4.5/6.0/8.5) of the 1 GCM, the variations of 93–98 are found for the total numbers of socioeconomic drought events, and the mean value of the total numbers is 96, which is a little smaller than those from the 16 AR4 GCMs. Moreover, the extreme socioeconomic drought events (i.e., SEDI = 4) will only account for a small percentage under all the 52 datasets, and the overall percentages of extreme socioeconomic drought events are 11% and 1% for the 16 AR4 GCMs and the 1 AR5 GCM, respectively. Regarding severe socioeconomic drought events (i.e., SEDI = 3) in future, the overall percentages are 35% and 55% for the 16 AR4 GCMs and the 1 AR5 GCM, respectively. As mentioned before, the GCM outputs can be used to analyze multi-decadal climate variations rather than to give the exact occurrence period of a drought event (Teegavarapu, 2012); therefore, the identified drought periods are for reference only. For example, an extreme socioeconomic drought event (i.e., SEDI = 4) is identified in 2079–2080 under RCP 8.5 scenario; it can only be inferred that there might be an extreme socioeconomic drought event during 2020–2099; however, the exact occurrence period of this event might be in other years rather than in 2079–2080.

Second, for each of the 52 datasets, the socioeconomic drought event with the longest drought duration in future is identified (see Fig. 7). It is observed that the values of the longest drought duration identified from the AR4 GCMs are generally larger than those identified from the AR5 GCM. The mean value of the longest drought duration identified from the AR4 GCMs is 33 months, and specially, the socioeconomic drought event identified from one AR4 GCM (i.e., csiro_mk3_0.1) under A1B scenario will last for 93 months (nearly 8 years), which is rather a long time. Moreover, the RSP value of this event is 3.05, indicating that there will be a desperate water shortage during that period. Known from Table 3, a decreasing trend in the simulated annual streamflow can be detected under this scenario, which may partly explain this situation. In contrast, the mean value of the longest drought duration identified from the AR5 GCM is only 14 months, much smaller than that identified from the AR4 GCMs, and the longest drought durations are 13, 12, 21 and 11 under RCP 2.6, 4.5, 6.0 and 8.5 scenarios, respectively. It indicates that, compared to the 16 AR4 GCMs, the selected 1 AR5 GCM will estimate future drought with a more optimistic view from the aspect of drought duration. In addition, the values of the longest drought duration identified from the 52 datasets are all larger than 9 months, which is the drought duration of the 1963 drought event identified from the simulated streamflow data.

Third, with reference to water shortage which is also a crucial factor, the largest RSP value under each of the 52 datasets is listed in Table 4. For the 16 AR4 GCMs, the largest RSP values vary between 0.91–2.53 under SRES B1 scenario, 0.91–3.05 under SRES A1B scenario and 0.94–2.39 under SRES A2 scenario, respectively, and the mean values under these three SRES scenarios are 1.49, 1.62 and 1.89, respectively. For the 1 AR5 GCM, the largest RSP values are 0.69, 0.77, 0.82 and 0.86 under RCP 2.6, 4.5, 6.0 and 8.5 scenarios, respectively. As a result, even the worst situation derived from the 1 AR5 GCM (i.e., 0.86) is better than the best situation derived from the 16 AR4 GCMs (i.e., 0.91), which indicates that, compared to the 16 AR4 GCMs, the selected 1 AR5 GCM will estimate future drought with a more optimistic view from the aspect of water shortage, which is the same as the result from the analysis of drought duration.

Conclusively, Table 5 lists the number of socioeconomic drought events with either longer duration or larger RSP value than the 1963 drought event identified from the simulated streamflow data during 2020–2099 for each of the 52 datasets, and the percentage in the parentheses is calculated by dividing the total number of socioeconomic drought events for the corresponding dataset. For the 16 AR4 GCMs, the numbers of such events vary between 16–39 under SRES A1B scenario, 18–39 under SRES A2 scenario and 22–39 under SRES B1 scenario, respectively. In future, socioeconomic drought events severer than the 1963 drought event will account for about 31% of the total. In contrast, for the four RCP scenarios (i.e., RCP 2.6/4.5/6.0/8.5) of the 1 AR5 GCM, smaller variations are found for the numbers of socioeconomic drought events severer than the 1963 drought event (i.e., 7–11), and the percentage of such events is about 9%, which once again proves the previous conclusion that the future drought condition estimated by the selected 1 AR5 GCM will be more optimistic than that estimated by the 16 AR4 GCMs.

4.4. Impact of the XFJ Reservoir

In the previous subsection, a number of socioeconomic drought events with different SEDI values have been identified in the East River basin. Therefore, serious water scarcity will be most likely to occur, especially if proper planning, development and management strategies are not adopted. For much of the 20th century, dam construction is regarded as the best option to increase available water resources

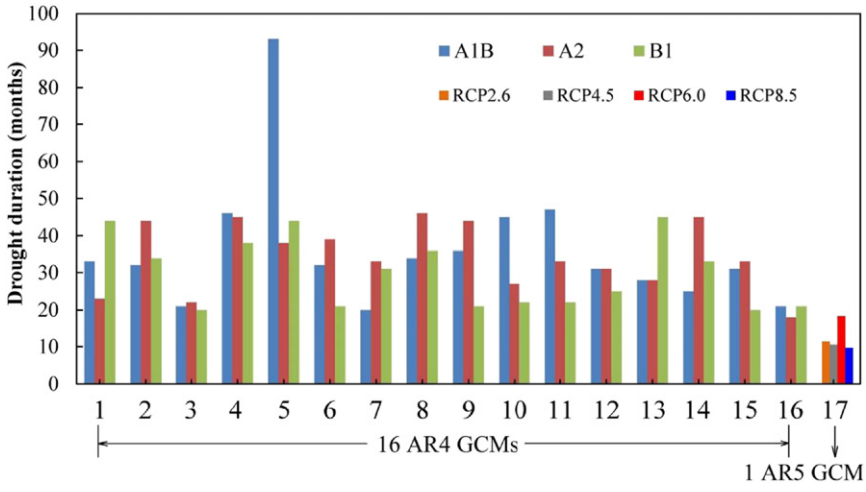

Fig. 7. Socioeconomic drought event with the longest drought duration for each of the 52 datasets.

Table 4
The largest RSP value during 2020–2099 for each of the 52 datasets.

AR4 scenario	A1B	A2	B1
1. bccr_bcm2_0.1	1.48	2.04	1.36
2. ncar_ccsm3_0.1	1.38	2.26	1.83
3. cccma_cgcm3_1.1	1.07	1.64	1.40
4. cnrm_cm3.1	2.85	2.39	1.60
5. csiro_mk3_0.1	3.05	2.22	1.81
6. mpi_echam5.1	1.80	2.26	1.02
7. miub_echo_g.1	0.91	2.07	1.27
8. gfdl_cm2_0.1	1.48	1.93	2.03
9. gfdl_cm2_1.1	1.59	2.05	1.34
10. giss_model_e_r.1/2	1.63	1.39	1.14
11. inmcm3_0.1	1.99	1.99	1.74
12. ipsl_cm4.1	1.17	1.36	1.40
13. miroc3_2_medres.1	1.49	1.99	2.53
14. mri_cgcm2_3_2a.1	1.55	2.00	1.57
15. ncar_pcm1.1/2	1.32	1.72	0.91
16. ukmo_hadcm3.1	1.11	0.94	0.93
Mean of the 16 AR4 GCMs	1.62	1.89	1.49

AR5 scenario	RCP 2.6	RCP 4.5	RCP 6.0	RCP 8.5
17. HadGEM2-ES	0.69	0.77	0.82	0.86

by storing water in the reservoir and enhance the capabilities in water resources management (Wu and Chen, 2012, 2013; Chen et al., 2016). Fortunately, a multi-year reservoir, the XFJ Reservoir, was completed in 1962 in the East River basin. Wu and Chen (2012) indicated that the usable capacity of the XFJ Reservoir was 5.8–6.5 km^3, which implied that at least nearly 90% of the effective storage (i.e., 6.5 km^3) of the XFJ Reservoir would be used to store water in the flood season. This study adopts 5.8 km^3 as the TRS for the East River basin, which is 0.89 (= 5.8/6.5) of the total effective storage, as the usable capacity (i.e., the available water volume) in the XFJ Reservoir when the flood season ends.

The monthly streamflow data simulated using the 52 datasets are used to analyze the impact of the XFJ Reservoir on future drought for the period of 2020–2099. Using the method described in Section 2.1, the available water volume in the XFJ Reservoir at the end of each month during 2020–2099 can be calculated. For the selected 1 AR5 GCM, without the reservoir, the largest RSP value under the four scenarios is 0.86 (see Table 4), which is smaller than 0.89; it indicates that the usable capacity (5.8 km^3) of the XFJ Reservoir is sufficient to cover the largest cumulative water deficit. However, for the 16 AR5 GCMs, with the reservoir, even the smallest RSP value (i.e., 0.91) in Table 4 is larger than 0.89, which means that water deficits will still remain in certain periods even if the adopted usable capacity is run out.

Fig. 8 shows the monthly available water volume in the XFJ Reservoir during 2020–2099 under three representative scenarios, namely, RCP 8.5 scenario with the largest RSP value of 0.86 (HadGEM2-ES), SRES A1B scenario with the largest RSP value of 1.11 (ukmo_hadcm3.1) and SRES B1 scenario with the largest RSP value of 1.40 (ipsl_cm4.1). The red dash lines denote that the usable capacity of the XFJ Reservoir (i.e., 5.8 km^3) is run out. For RCP 8.5 scenario (HadGEM2-ES), the usable capacity of the XFJ Reservoir will be sufficient for future water demand (see Fig. 8a), For SRES A1B scenario (ukmo_hadcm3.1) and SRES B1 scenario (ipsl_cm4.1), there are several drought events whose water deficits cannot be completely tackled by the usable capacity of the XFJ Reservoir (see Fig. 8b and c).

Furthermore, it is worth noting that the available water volume in the XFJ Reservoir at the end of the flood season is usually <5.8 km^3, which will have a great influence on future drought analysis. Therefore, relationship between the number of socioeconomic drought events and the used percentage of the effective storage of the XFJ Reservoir is discussed, taking the 1 AR5 GCM under the four RCP scenarios during 2020–2099 as a case study, and the relevant results are shown in

Table 5
The number of socioeconomic drought events with either longer duration or larger RSP value than the 1963 drought event during 2020–2099 for each of the 52 datasets. Note: the percentages in the parentheses are calculated by dividing the total number of socioeconomic drought events for the corresponding dataset.

AR4 scenario	A1B	A2	B1
1. bccr_bcm2_0.1	29 (28%)	27 (24%)	35 (34%)
2. ncar_ccsm3_0.1	28 (25%)	32 (37%)	32 (30%)
3. cccma_cgcm3_1.1	28 (25%)	30 (28%)	22 (20%)
4. cnrm_cm3.1	38 (45%)	29 (34%)	31 (34%)
5. csiro_mk3_0.1	29 (32%)	34 (37%)	31 (33%)
6. mpi_echam5.1	33 (31%)	35 (36%)	37 (38%)
7. miub_echo_g.1	32 (31%)	33 (31%)	28 (28%)
8. gfdl_cm2_0.1	33 (33%)	31 (32%)	26 (26%)
9. gfdl_cm2_1.1	33 (31%)	32 (34%)	26 (25%)
10. giss_model_e_r.1/2	27 (24%)	18 (15%)	25 (22%)
11. inmcm3_0.1	33 (37%)	39 (45%)	39 (39%)
12. ipsl_cm4.1	31 (32%)	35 (42%)	38 (37%)
13. miroc3_2_medres.1	34 (39%)	33 (32%)	27 (29%)
14. mri_cgcm2_3_2a.1	39 (38%)	36 (40%)	33 (31%)
15. ncar_pcm1.1/2	32 (38%)	31 (31%)	30 (27%)
16. ukmo_hadcm3.1	16 (15%)	19 (16%)	27 (25%)
Mean of the 16 AR4 GCMs	31 (31%)	31 (32%)	30 (30%)

AR5 scenario	RCP 2.6	RCP 4.5	RCP 6.0	RCP 8.5
17. HadGEM2-ES	7 (7%)	7 (7%)	9 (9%)	11 (12%)

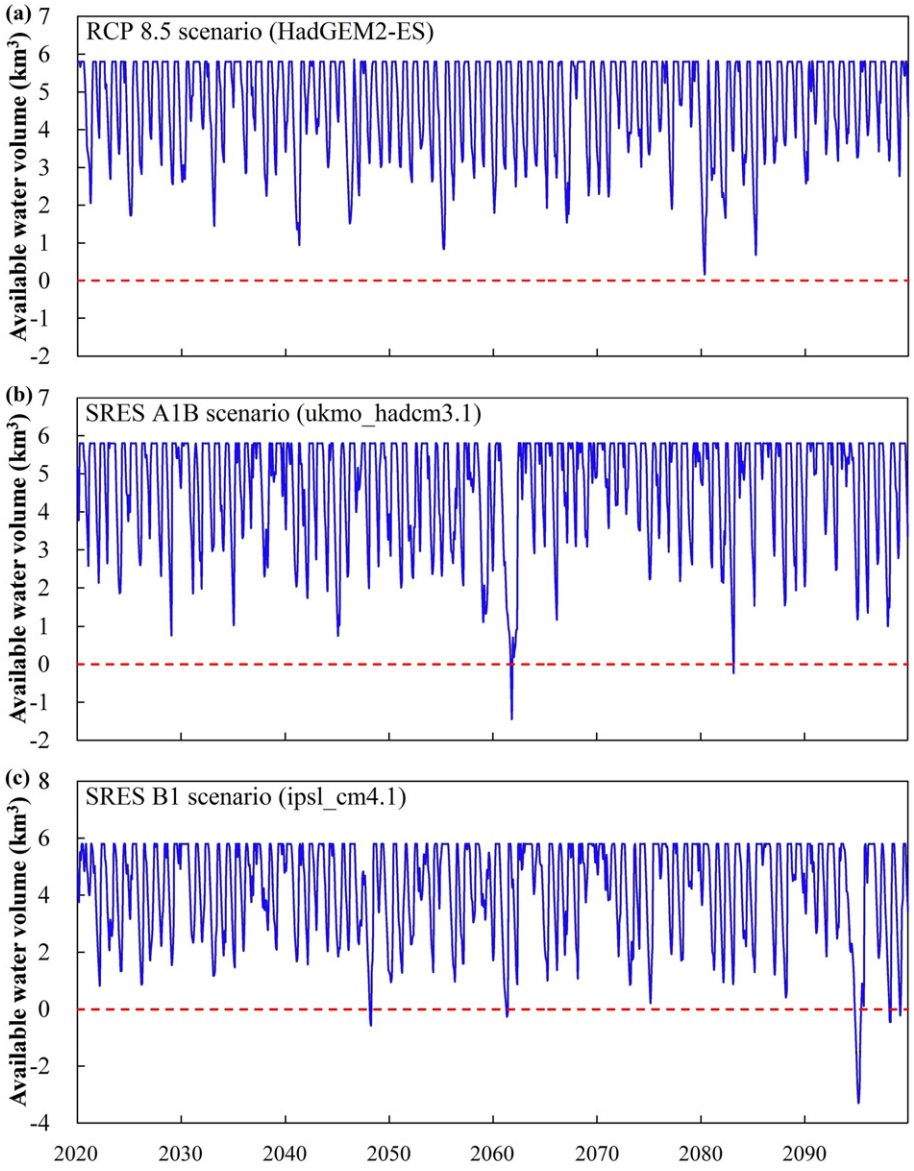

Fig. 8. The monthly available water volume in the XFJ Reservoir during 2020–2099 under three representative scenarios. Note: the red dash lines denote the usable capacity of the XFJ Reservoir (i.e., 5.8 km^3) is run out.

Fig. 9 and Table 6. Along with the increase of the used percentage of the effective storage, the total number of socioeconomic drought events will monotonously decrease under all these four scenarios; however, the decreasing trends can be divided into three phases, with quite different decreasing features. Since the step of the used percentage for this analysis is 10%, the first cutoff point is found between 20% and 30% while the second cutoff point is found between 60% and 70% (see Fig. 9). When no >20% of the effective storage is used, the average trend slope for all these four scenarios is −0.94 ($R^2 = 0.85$), which is much weaker than that (i.e., −2.08, $R^2 = 0.96$) when the used percentage is between 30% and 60%. Moreover, when no <70% of the effective storage is used, the decreasing trend becomes quite weak (i.e., −0.11, $R^2 = 0.48$) mainly because the total number of socioeconomic drought events is small. As a result, to reserve 70% of the effective storage of the XFJ Reservoir at the end of the flood season can be a good option because most socioeconomic drought events will be overcome in that case. In addition, regarding the number of socioeconomic drought events with different SEDI values (see Table 6), when no <30% of the effective storage is used, most socioeconomic drought events on severe (i.e., SEDI = 3)

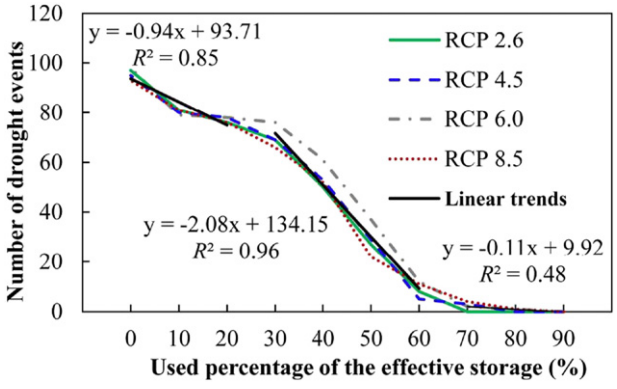

Fig. 9. The relationship between the number of socioeconomic drought events and the used percentage of the effective storage of the XFJ Reservoir based on the 1 AR5 GCM under the four scenarios during 2020–2099. Note: the black lines denote the linear trends.

Table 6
The numbers of socioeconomic drought events when different percent of the effective storage of the XFJ Reservoir is used under each of the 4 scenarios of the 1 AR5 GCM.

Used percent	Total	SEDI = 1	SEDI = 2	SEDI = 3	SEDI = 4	Total	SEDI = 1	SEDI = 2	SEDI = 3	SEDI = 4
	RCP 2.6 scenario					RCP 4.5 scenario				
0	97	19	24	53	1	95	16	25	54	0
10%	81	8	37	36	0	80	3	44	33	0
20%	76	16	48	12	0	78	18	51	9	0
30%	69	30	27	2	0	69	36	30	3	0
40%	50	34	16	0	0	53	35	17	1	0
50%	27	24	3	0	0	29	24	5	0	0
60%	8	8	0	0	0	5	4	1	0	0
70%	0	0	0	0	0	3	3	0	0	0
80%	0	0	0	0	0	0	0	0	0	0
90%	0	0	0	0	0	0	0	0	0	0
	RCP 6.0 scenario					RCP 8.5 scenario				
0	98	21	20	55	2	93	16	27	49	1
10%	79	4	39	35	1	81	9	44	28	0
20%	78	14	53	11	0	76	18	44	14	0
30%	76	33	40	3	0	66	33	27	6	0
40%	61	37	22	0	0	52	37	14	1	0
50%	37	33	4	0	0	22	15	7	0	0
60%	12	12	0	0	0	11	8	3	0	0
70%	2	2	0	0	0	4	4	0	0	0
80%	1	1	0	0	0	1	1	0	0	0
90%	0	0	0	0	0	0	0	0	0	0

and extreme (i.e., SEDI = 4) levels will be removed. For example, when the used percentage is 30%, there will be no extreme socioeconomic drought events during 2020–2099, and only 2, 3, 3, and 6 severe socioeconomic drought events are remaining under these four RCP scenarios, respectively. Consequently, for the climate change circumstances provided by the 1 AR5 GCM, we would suggest to reserve at least 30% of the effective storage of the XFJ Reservoir at the end of the flood season.

5. Conclusions

This study proposes a new method (i.e., a heuristic method) and a new index (i.e., the SEDI) for identifying socioeconomic drought events on different severity levels under climate change through comprehensively evaluating the impacts of both water shortage and drought duration. Taking the East River basin in South China as the study area, this study analyzes both the historical and future socioeconomic drought events using the proposed method and index. The contributions of this study can be described as follows:

First, the MWR value of the East River basin for each year during 2010–2099 is obtained through considering the change of water demand in future, which can be a target of the integrated water resources management in this river basin and a reference to other river basins. Second, the SEDI is validated through historical drought analysis, and then applied to future drought analysis. The trends of the simulated streamflow derived from 52 datasets are analyzed, and socioeconomic drought events during 2020–2099 are identified. The results indicate that a number of socioeconomic drought events severer than the 1963 drought event may occur in future, which will be a great challenge for the society. Third, through analyzing the impact of the XFJ Reservoir on future droughts, this study indicates that most of the identified socioeconomic drought events can be mitigated by reservoir operation if the used percentage of the effective storage at the end of the flood season is 70%. Moreover, it is suggested that at least 30% of the effective storage should be reserved in the XFJ Reservoir at the end of the flood season to overcome most of the severe and extreme socioeconomic drought events.

Furthermore, applying the proposed method and index for identifying socioeconomic drought events under climate change, we also need fully aware the following limitations, which are mainly related to five aspects. First, one important indicator to develop the SEDI is the RSP, in which the effective reservoir storage is a necessary variable. Therefore, the heuristic method and the SEDI are inapplicable to river basins without reservoir operation. Fortunately, reservoir seems to be the requisite infrastructure in river basins where socioeconomic drought events may occur because reservoir can definitely enhance the capabilities in meeting water demand (Chen et al., 2016). Second, the proposed method and index are region-dependent. The study area is located in a humid region, and the method and index are applicable. For arid or semi-arid regions, more water-related factors (e.g., utilization of groundwater) besides streamflow may have to be considered, and the method and index may need more validations. Nevertheless, the proposed method and index may interpret the occurrence of drought event in arid or semi-arid regions from the perspective of water supply and demand, rather than only from the perspective of climatology. Moreover, for different regions, relationship between the number of socioeconomic drought events and the used percentage of the effective storage should be reestablished and suggestion about the used percentage of the effective storage may be different. Third, this study adopts the simulation results of a semi-distributed model (i.e., the VIC model) over a relatively coarse resolution spatial grid, which may simplify the description of the behavior of spatially distributed physical systems and may bring in errors. Distributed hydrological models can be used in the future work to further analyze the possible influences of different models on the proposed method and index. Fourth, the missing data will influence the computation of the SEDI. Nevertheless, this study uses the simulated streamflow from the VIC model, and there is no missing data. Fifth, it is worth noting that IPCC is still intensively monitoring and studying climate change and new climate change projections will be issued in the next several years. Therefore, the performance of the proposed method and index should be re-evaluated when the new systematic projections are available.

Nevertheless, with the awareness of the above limitations, the heuristic method and the SEDI proposed in this study can provide a new avenue of identifying socioeconomic drought events under climate change, which would be valuable for sustainable water resources management. It is worth noting that the proposed new method and index would be promising in other humid regions with reservoir operation around the world. Even if in arid or semi-arid regions, the proposed new method and index can be regarded as a pilot exploration of understanding drought events from a socioeconomic perspective.

Acknowledgements

This study was supported by the Consultancy Services project for Water Supplies Department of Hong Kong "Study on impacts of climate change on the water resources of Hong Kong", the Natural Science Foundation of Qinghai Province project (Grant No. 2017-ZJ-911), and the Special Funding for Science and Technology Development in Guangdong Province (Grant No. 2016A050503035). We are also grateful to the two anonymous reviewers and Associate Editor (Prof. Wei Ouyang) who offered the insightful and constructive comments leading to improvement of this paper.

References

Adam, J.C., Lettenmaier, D.P., 2003. Adjustment of global gridded precipitation for systematic bias. J. Geophys. Res. 108, 1–14.
Aherne, J., Larssen, T., Cosby, B.J., Dillon, P.J., 2006. Climate variability and forecasting surface water recovery from acidification: modelling drought-induced sulphate release from wetlands. Sci. Total Environ. 365, 186–199.
Ahn, S.R., Jeong, J.H., Kim, S.J., 2016. Assessing drought threats to agricultural water supplies under climate change by combining the SWAT and MODSIM models for the Geum River basin, South Korea. Hydrol. Sci. J. 61 (15), 2740–2753.
American Meteorological Society, 2013. Drought - An Information Statement of the American Meteorological Society. https://www.ametsoc.org/ams/index.cfm/about-ams/ams-statements/statements-of-the-ams-in-force/drought/.
Cammalleri, C., Vogt, J., Salamon, P., 2017. Development of an operational low-flow index for hydrological drought monitoring over Europe. Hydrol. Sci. J. 62 (3), 346–358.

Chan, H., Kok, M., Lee, T., 2012. Temperature trends in Hong Kong from a seasonal perspective. Clim. Res. 55 (1), 53–63.
Chen, J., Wu, Y.P., 2008. Exploring hydrological process features of the East River (Dongjiang) basin in South China using VIC and SWAT. Proceedings of the International Association of Hydrological Sciences and the International Water Resources Association Conference, Guangzhou, China, pp. 8–10.
Chen, J., Li, Q.L., Niu, J., Sun, L.Q., 2011. Regional climate change and local urbanization effects on weather variables in Southeast China. Stoch. Env. Res. Risk A. 25 (4), 555–565.
Chen, J., Xing, B.D., Shi, H.Y., Zhang, B., 2015. A new model for long-term global water demand projection. AGU Fall Meeting, San Francisco, USA.
Chen, J., Shi, H.Y., Sivakumar, B., Peart, M.R., 2016. Population, water, food, energy and dams. Renew. Sust. Energ. Rev. 56, 18–28.
Croitoru, A.E., Holobaca, I.H., Lazar, C., Moldovan, F., Imbroane, A., 2012. Air temperature trend and the impact on winter wheat phenology in Romania. Clim. Chang. 111 (2), 393–410.
Denver Water, 2002. Water for Tomorrow: An Integrated Water Resource Plan.
Eklund, L., Seaquist, J., 2015. Meteorological, agricultural and socioeconomic drought in the Duhok Governorate, Iraqi Kurdistan. Nat. Hazards 76 (1), 421–441.
Etienne, E., Devineni, N., Khanbilvardi, R., Lall, U., 2016. Development of a demand sensitive drought index and its application for agriculture over the conterminous United States. J. Hydrol. 534, 219–229.
Fischer, T., Menz, C., Su, B., Scholten, T., 2013. Simulated and projected climate extremes in the Zhujiang River Basin, South China, using the regional climate model COSMO-CLM. Int. J. Climatol. 33, 2988–3001.
Gan, T.Y., Ito, M., Hulsmann, S., Qin, X., Lu, X.X., Liong, S.Y., Rutschman, P., Disse, M., Koivusalo, H., 2016. Possible climate change/variability and human impacts, vulnerability of drought-prone regions, water resources and capacity building for Africa. Hydrol. Sci. J. 61 (7), 1209–1226.
Gizaw, M.S., Gan, T.Y., 2017. Impact of climate change and El Nio episodes on droughts in sub-Saharan Africa. Clim. Dyn. 49 (1–2), 665–682.
Gu, H.H., Yu, Z.B., Wang, G.L., Wang, J.G., Ju, Q., Yang, C.G., Fan, C.H., 2015. Impact of climate change on hydrological extremes in the Yangtze River Basin, China. Stoch. Env. Res. Risk A. 29 (3), 693–707.
Guttman, N.B., 1998. Comparing the Palmer Drought index and the standardized precipitation index. American Water Resources Association]–>J. Am. Water Resour. Assoc. 34 (1), 113–121.
Hanson, P.J., Weltzin, J.F., 2000. Drought disturbance from climate change: response of United States forests. Sci. Total Environ. 262 (3), 205–220.
Heim, R.R., 2002. A review of twentieth-century drought indices used in the United States. American Meteorological Society]–>Bull. Am. Meteorol. Soc. 83, 1149–1166.
Hirabayashi, Y., Kanae, S., Emori, S., Oki, T., Kimoto, M., 2008. Global projections of changing risks of floods and droughts in a changing climate. Hydrol. Sci. J. 53 (4), 754–772.
Hoang, L.P., Lauri, H., Kummu, M., Koponen, J., van Vliet, M.T.H., Supit, I., Leemans, R., Kabat, P., Ludwig, F., 2016. Mekong River flow and hydrological extremes under climate change. Hydrol. Earth Syst. Sci. 20 (7), 3027–3041.
Huang, S.Z., Huang, Q., Leng, G.Y., Liu, S.Y., 2016. A nonparametric multivariate standardized drought index for characterizing socioeconomic drought: a case study in the Heihe River Basin. J. Hydrol. 542, 875–883.
IPCC, 2007. Climate Change 2007: The Physical Science Basis. Contribution of Working Group I to the Fourth Assessment Report of the IPCC. Cambridge University Press, Cambridge, United Kingdom and New York, USA.
IPCC, 2013. Climate Change 2013: The Physical Science Basis. Contribution of Working Group I to the Fifth Assessment Report of the IPCC. Cambridge University Press, Cambridge, United Kingdom and New York, USA.
Juhasz, T., Kornfield, J., 1978. The crop moisture index: unnatural response to changes in temperature. J. Appl. Meteorol. Climatol. 17, 1864–1865.
Karl, T.R., 1986. The sensitivity of the Palmer Drought severity index and Palmer's Z-index to their calibration coefficients including potential evapotranspiration. J. Clim. Appl. Meteorol. 25, 77–86.
Kendall, M.G., 1975. Rank Correlation Measures. Charles Griffin, London.
Kifer, R.S., Steward, H.L., 1938. Farming hazards in the drought area. Monograph XVI. Works Progress Administration, Washington, DC.
Kogan, F.N., 1995. Droughts of the late 1980s in the United States as derived from NOAA polar-orbiting satellite data. American Meteorological Society]–>Bull. Am. Meteorol. Soc. 76, 655–668.
Lau, K.L., Ng, E., 2013. An investigation of urbanization effect on urban and rural Hong Kong using a 40-year extended temperature record. Landsc. Urban Plan. 114, 42–52.
Lee, J.H.W., Wang, Z.Y., Thoe, W., Cheng, D.S., 2007. Integrated physical and ecological management of the East River. Water Sci. Technol. Water Supply 7, 81–91.
Liang, X., Lettenmaier, D.P., Wood, E.F., Burges, S.J., 1994. A simple hydrologically based model of land surface water and energy fluxes for general circulation models. J. Geophys. Res. 99 (D7), 14415–14428.
Lin, Q.X., Wu, Z.Y., Singh, V.P., Sadeghi, S.H.R., He, H., Lu, G.H., 2017. Correlation between hydrological drought, climatic factors, reservoir operation, and vegetation cover in the Xijiang Basin, South China. J. Hydrol. 549, 512–524.
Linares, R., Roque, C., Gutierrez, F., Zarroca, M., Carbonel, D., Bach, J., Fabregat, I., 2017. The impact of droughts and climate change on sinkhole occurrence. A case study from the evaporite karst of the Fluvia Valley, NE Spain. Sci. Total Environ. 579, 345–358.
Mann, H.B., 1945. Non-parametric tests against trend. Econometrica 13, 245–259.
Manzanas, R., Amekudzi, L.K., Preko, K., Herrera, S., Gutierrez, J.M., 2014. Precipitation variability and trends in Ghana: an intercomparison of observational and reanalysis products. Clim. Chang. 124 (4), 805–819.
Maurer, E.P., Adam, J.C., Wood, A.W., 2009. Climate model based consensus on the hydrologic impacts of climate change to the Rio Lempa basin of Central America. Hydrol. Earth Syst. Sci. 13, 183–194.
McKee, T.B., Doesken, N.J., Kleist, J., 1993. The relationship of drought frequency and duration to time scales. Eighth Conference on Applied Climatology. American Meteorological Society, Anaheim, California.
Meehl, G.A., Covey, C., Delworth, T., Latif, M., McAvaney, B., Mitchell, J.F.B., Stouffer, R.J., Taylor, K.E., 2007. The WCRP CMIP3 multi-model dataset: a new era in climate change research. American Meteorological Society]–>Bull. Am. Meteorol. Soc. 88, 1383–1394.
Mehran, A., Mazdiyasni, O., AghaKouchak, A., 2015. A hybrid framework for assessing socioeconomic drought: linking climate variability, local resilience, and demand. J. Geophys. Res.-Atmos. 120 (15), 7520–7533.
Mishra, A.K., Singh, V.P., 2010. A review of drought concepts. J. Hydrol. 391, 202–216.
Moorhead, J.E., Gowda, P.H., Singh, V.P., Porter, D.O., Marek, T.H., Howell, T.A., Stewart, B.A., 2015. Identifying and evaluating a suitable index for agricultural drought monitoring in the Texas high plains. American Water Resources Association]–>J. Am. Water Resour. Assoc. 51 (3), 807–820.
Morán-Tejeda, E., Ceglar, A., Medved-Cvikl, B., Vicente-Serrano, S.M., López-Moreno, J.I., González-Hidalgo, J.C., Revuelto, J., Lorenzo-Lacruz, J., Camarero, J., Pasho, E., 2013. Assessing the capability of multi-scale drought datasets to quantify drought severity and to identify drought impacts: an example in the Ebro Basin. Int. J. Climatol. 33 (8), 1884–1897.
Narasimhan, B., Srinivasan, R., 2005. Development and evaluation of soil moisture deficit index (SMDI) and evapotranspiration deficit index (ETDI) for agricultural drought monitoring. Agric. For. Meteorol. 133 (1–4), 69–88.
Ndehedehe, C.E., Awange, J.L., Corner, R.J., Kuhn, M., Okwuashi, O., 2016. On the potentials of multiple climate variables in assessing the spatio-temporal characteristics of hydrological droughts over the Volta Basin. Sci. Total Environ. 557, 819–837.
Nijssen, B., Schnur, R., Lettenmaier, D.P., 2001. Global retrospective estimation of soil moisture using the Variable Infiltration Capacity land surface model, 1980–93. J. Clim. 14 (8), 1790–1808.
Niu, J., 2013. Precipitation in the Pearl River basin, South China: scaling, regional patterns, and influence of large-scale climate anomalies. Stoch. Env. Res. Risk A. 27 (5), 1253–1268.
Niu, J., Chen, J., 2010. Terrestrial hydrological features of the Pearl River basin in South China. J. Hydro Environ. Res. 4 (4), 279–288.
Niu, J., Chen, J., 2014. Terrestrial hydrological responses to precipitation variability in Southwest China with emphasis on drought. Hydrol. Sci. J. 59 (2), 325–335.
Niu, J., Chen, J., 2016. A wavelet perspective on variabilities of hydrological processes in conjunction with geomorphic analysis over the Pearl River basin in South China. J. Hydrol. 542, 392–409.
Niu, J., Chen, J., Sivakumar, B., 2014. Teleconnection analysis of runoff and soil moisture over the Pearl River basin in South China. Hydrol. Earth Syst. Sci. 18 (4), 1475–1492.
Niu, J., Chen, J., Sun, L.Q., 2015. Exploration of drought evolution using numerical simulations over the Xijiang (West River) basin in South China. J. Hydrol. 526, 68–77.
Niu, J., Chen, J., Wang, K.Y., Sivakumar, B., 2017. Multi-scale streamflow variability responses to precipitation over the headwater catchments in southern China. J. Hydrol. 551, 14–28.
Palmer, W.C., 1965. Meteorological drought. U.S. Weather Bureau. 45, p. 58.
Palmer, W.C., 1968. Keeping track of crop moisture conditions, nationwide: the new crop moisture index. Weatherwise 21, 156–161.
Peart, M.R., 2004. Water supply and the development of Hong Kong. Proceedings of the UNESCO/IAHS/IWHA Symposium, pp. 23–30.
Pilling, C.G., Jones, J.A.A., 2002. The impact of future climate change on seasonal discharge, hydrological processes and extreme flows in the Upper Wye experimental catchment, mid-Wales. Hydrol. Process. 16 (6), 1201–1213.
PRWRC (Pearl River Water Resources Commission), 2005. Pearl River Flood Prevention Handbook (in Chinese).
Sen, P.K., 1968. Estimates of the regression coefficient based on Kendall's tau. American Statistical Association]–>J. Am. Stat. Assoc. 63, 1379–1389.
Serinaldi, F., 2016. Can we tell more than we can know? The limits of bivariate drought analyses in the United States. Stoch. Env. Res. Risk A. 30 (6), 1691–1704.
Shafer, B.A., Dezman, L.E., 1982. Development of a Surface Water Supply Index (SWSI) to assess the severity of drought conditions in snowpack runoff areas. Proceedings of the Western Snow Conference. 50, pp. 164–175.
Shi, H.Y., Wang, G.Q., 2015. Impacts of climate change and hydraulic structures on runoff and sediment discharge in the middle Yellow River. Hydrol. Process. 29 (14), 3236–3246.
Shi, H.Y., Li, T.J., Wei, J.H., Fu, W., Wang, G.Q., 2016a. Spatial and temporal characteristics of precipitation over the Three-River Headwaters region during 1961–2014. J. Hydrol. 6, 52–65.
Shi, H.Y., Li, T.J., Wang, K., Zhang, A., Wang, G.Q., Fu, X.D., 2016b. Physically based simulation of the streamflow decrease caused by sediment-trapping dams in the middle Yellow River. Hydrol. Process. 30 (5), 783–794.
Shi, H.Y., Li, T.J., Wang, G.Q., 2017a. Temporal and spatial variations of potential evaporation and the driving mechanism over Tibet during 1961–2001. Hydrol. Sci. J. 62 (9), 1469–1482.
Shi, H.Y., Li, T.J., Wei, J.H., 2017b. Evaluation of the gridded CRU TS precipitation dataset with the point raingauge records over the Three-River Headwaters region. J. Hydrol. 548, 322–332.
Shukla, S., Wood, A.W., 2008. Use of a standardized runoff index for characterizing hydrologic drought. Geophys. Res. Lett. 35 (2), L02405.
Sivakumar, M.V.K., Motha, R.P., Wilhite, D.A., Wood, D.A., 2011. Agricultural Drought Indices. Proceedings of the WMO/UNISDR Expert Group Meeting on Agricultural Drought Indices, Murcia, Spain.
Smirnov, O., Zhang, M.H., Xiao, T.Y., Orbell, J., Lobben, A., Gordon, J., 2016. The relative importance of climate change and population growth for exposure to future extreme droughts. Clim. Chang. 138 (1–2), 41–53.

Teegavarapu, R.S.V., 2012. Floods in a Changing Climate: Extreme Precipitation. Cambridge University Press, New York, USA.
Thiel, H., 1950. A rank-invariant method of linear and polynomial regression analysis, III. Proceedings of Koninalijke Nederlandse Akademie van Weinenschatpen. 53, pp. 1397–1412.
Tietjen, B., Schlaepfer, D.R., Bradford, J.B., Lauenroth, W.K., Hall, S.A., Duniway, M.C., Hochstrasser, T., Jia, G., Munson, S.M., Pyke, D.A., Wilson, S.D., 2017. Climate change-induced vegetation shifts lead to more ecological droughts despite projected rainfall increases in many global temperate drylands. Glob. Chang. Biol. 23 (7), 2743–2754.
Trinh, T., Ishida, K., Kavvas, M.L., Ercan, A., Carr, K., 2017. Assessment of 21st century drought conditions at Shasta Dam based on dynamically projected water supply conditions by a regional climate model coupled with a physically-based hydrology model. Sci. Total Environ. 586, 197–205.
United Nations (UN), 1997. Comprehensive Assessment of the Freshwater Resources of the World. http://www.un.org/esa/documents/ecosoc/cn17/1997/ecn171997-9.htm.
Vicente-Serrano, S.M., Beguería, S., López-Moreno, J.I., 2010. A multi-scalar drought index sensitive to global warming: the standardized precipitation evapotranspiration index - SPEI. J. Clim. 23 (7), 1696–1718.
Vicuna, S., Gironas, J., Meza, F.J., Cruzat, M.L., Jelinek, M., Bustos, E., Poblete, D., Bambach, N., 2013. Exploring possible connections between hydrological extreme events and climate change in central south Chile. Hydrol. Sci. J. 58 (8), 1598–1619.
von Storch, H., Navarra, A., 1995. Analysis of Climate Variability: Applications of Statistical Techniques. Springer-Verlag, Berlin.
Wilhite, D.A., Glantz, M.H., 1985. Understanding the drought phenomenon: the role of definitions. Water Int. 10, 111–120.
Wood, A.W., Leung, L.R., Sridhar, V., Lettenmaier, D.P., 2004. Hydrologic implications of dynamical and statistical approaches to downscaling climate model outputs. Clim. Chang. 62, 189–216.
Wu, Y.P., Chen, J., 2012. An operation-based scheme for a multiyear and multipurpose reservoir to enhance macroscale hydrologic models. J. Hydrometeorol. 13 (1), 270–283.
Wu, Y.P., Chen, J., 2013. Estimating irrigation water demand using an improved method and optimizing reservoir operation for water supply and hydropower generation: a case study of the Xinfengjiang reservoir in southern China. Agric. Water Manag. 116, 110–121.
Wu, H.X., Zhang, Q.T., Zeng, W.H., 2001. Preliminary study of salt water in the Dongjiang delta. Guangdong Water Resour. Hydropower 5, 1–3 (in Chinese).
Wu, C.H., Xian, Z.Y., Huang, G.R., 2017. Meteorological drought in the Beijiang River basin, South China: current observations and future projections. Stoch. Env. Res. Risk A. 30 (7), 1821–1834.
Yoo, J., Kim, D., Kim, H., Kim, T.W., 2016. Application of copula functions to construct confidence intervals of bivariate drought frequency curve. J. Hydro Environ. Res. 11, 113–122.
Zuo, Q.T., 2011. Discussion on the calculation method and threshold of the net-utilization ratio of water resources. J. Hydraul. Eng. 42 (11), 1372–1378 (in Chinese).